

## Toroidal magnetic moments in $\text{Tb}_4$ squares

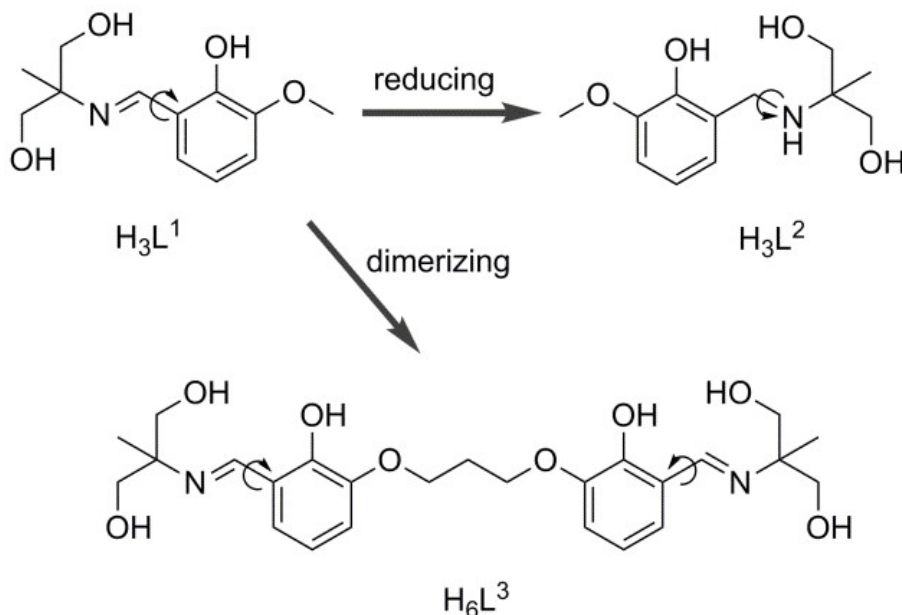
Qianqian Yang,<sup>a,b</sup> Liviu Ungur,<sup>\*c</sup> Wolfgang Wernsdorfer,<sup>d</sup> and Jinkui Tang<sup>\*a,b</sup>

<sup>a</sup>State Key Laboratory of Rare Earth Resource Utilization, Changchun Institute of Applied Chemistry, Chinese Academy of Sciences, Changchun 130022, P. R. China. E-mail: tang@ciac.ac.cn

<sup>b</sup>School of Applied Chemistry and Engineering, University of Science and Technology of China, Hefei 230026, P. R. China

<sup>c</sup>Department of Chemistry, National University of Singapore, 117543, Singapore. Email: chmlu@nus.edu.sg

<sup>d</sup>Institute of Quantum Materials and Technologies, KIT, D-76344, Eggenstein-Leopoldshafen, Germany



Scheme S1 Schematic drawing of the ligands  $\text{H}_3\text{L}^1$ ,  $\text{H}_3\text{L}^2$  (top), and  $\text{H}_6\text{L}^3$  (bottom).

Table S1. Crystallographic data for complexes **1-3**.

	<b>1</b>	<b>2</b>	<b>3</b>
Formula	$\text{C}_{58}\text{H}_{92}\text{N}_8\text{O}_{22}\text{S}_3\text{Tb}_4$	$\text{C}_{52}\text{H}_{72}\text{N}_6\text{O}_{23}\text{S}_2\text{Tb}_4$	$\text{C}_{56}\text{H}_{78}\text{Cl}_2\text{N}_6\text{O}_{21}\text{Tb}_4$
FW, g·mol <sup>-1</sup>	1985.25	1848.95	1877.82
crystal system	Triclinic	Triclinic	Monoclinic
space group	$P\bar{1}$	$P\bar{1}$	$P2_1/c$
$T$ , K	273(2)	273(2)	273(2)
$\lambda$ , Å	0.71073	0.71073	0.71073
$a$ , Å	10.3655(4)	10.1491(6)	13.0232(9)
$b$ , Å	13.8257(5)	12.5665(7)	17.6485(12)
$c$ , Å	27.5944(11)	13.2970(8)	15.8686(11)
$\alpha$ , °	83.4140(10)	87.4245(12)	90
$\beta$ , °	81.6150(10)	82.0759(12)	114.1920(10)
$\gamma$ , °	68.5730(10)	68.9009(12)	90

$V$ , Å <sup>3</sup>	3633.8(2)	1567.06(16)	3326.9(4)
Z	2	1	2
$\rho_{\text{calcd}}$ , g·cm <sup>-3</sup>	1.814	1.959	1.875
GOF on $F^2$	1.023	0.985	1.048
reflns collected	22758	9834	20774
$R_1$ ( $I \geq 2 \sigma(I)$ )	0.0419	0.0540	0.0430
$wR_2$ (all data)	0.1002	0.1422	0.1198
CCDC	1487722	1487721	1487723

Table S2 Selected bond distances (Å) and bond angles (°) for complexes **1-3**.

	Complex 1 (a, b)		Complex 2		Complex 3	
Tb1-O1	2.4818(2)	2.4749(3)	Tb1-O1	2.5473(5)	Tb1-O1	2.6159(4)
Tb2-O1	2.5115(3)	2.5193(5)	Tb2-O1	2.4711(5)	Tb2-O1	2.4360(3)
Average Tb-O	2.4966(5)	2.4971(5)	Average Tb-O	2.5092(5)	Average Tb-O	2.5260(5)
Tb1-Tb2	3.5392(4)	3.5349(8)	Tb1-Tb2	3.5499(7)	Tb1-Tb2	3.5797(5)
Tb1-Tb2#	3.5225(4)	3.5282(5)	Tb1-Tb2#	3.5480(7)	Tb1-Tb2#	3.5694(4)
Tb1-Tb1#	4.9637(6)	4.9498(6)	Tb1-Tb1#	5.0946(7)	Tb1-Tb1#	5.2319(5)
Tb2-Tb2#	5.0230(7)	5.0385(7)	Tb2-Tb2#	4.9423(7)	Tb2-Tb2#	4.8720(4)
Average Tb-Tb	3.5308(5)	3.5316(5)	Average Tb-Tb	3.5490(5)	Average Tb-Tb	3.5746(5)
Tb1-O1-Tb2	90.270(8)	90.108(1)	Tb1-O1-Tb2	89.970(2)	Tb1-O1-Tb2	90.166(1)
Tb1-O1-Tb2#	89.730(8)	89.892(1)	Tb1-O1-Tb2#	90.029(2)	Tb1-O1-Tb2#	89.834(1)
Average Tb-O-Tb	90	90	Average Tb-O-Tb	90	Average Tb-O-Tb	90
Tb1-O1-Tb1#	180	180	Tb1-O1-Tb1#	180	Tb1-O1-Tb1#	180
Tb2-O1-Tb2#	180	180	Tb2-O1-Tb2#	180	Tb2-O1-Tb2#	180
#: -x+1, -y+1, -z+1			-x+2, -y, -z+1			-x+1, -y+2, -z

Table S3 The CShM values calculated by *SHAPE* 2.1<sup>1</sup> for **1-3**.

Central atom	Coordination Geometry	Complex 1 (a, b)	Complex 2	Complex 3
Tb1	Square antiprism ( $D_{4d}$ )	2.647	2.339	3.238
	Triangular dodecahedron ( $D_{2d}$ )	2.762	2.569	2.423
	Johnson gyrobifastigium J26 ( $D_{2d}$ )	12.694	12.890	11.360
	Biaugmented trigonal prism J50 ( $C_{2v}$ )	2.391	2.303	3.070
	Biaugmented trigonal prism ( $C_{2v}$ )	2.190	2.149	2.787
	Snub diphenoid J84 ( $D_{2d}$ )	4.321	4.240	3.733
Tb2	Capped cube J8 ( $C_{4v}$ )	11.240	11.299	10.492
	Spherical-relaxed capped cube ( $C_{4v}$ )	10.523	10.654	9.374
	Capped square antiprism J10 ( $C_{4v}$ )	1.683	1.764	1.877
	Spherical capped square antiprism ( $C_{4v}$ )	1.053	1.116	0.961
	Tricapped trigonal prism J51 ( $D_{3h}$ )	1.341	1.326	2.288
	Spherical tricapped trigonal prism ( $D_{3h}$ )	0.775	0.726	0.987
				0.933

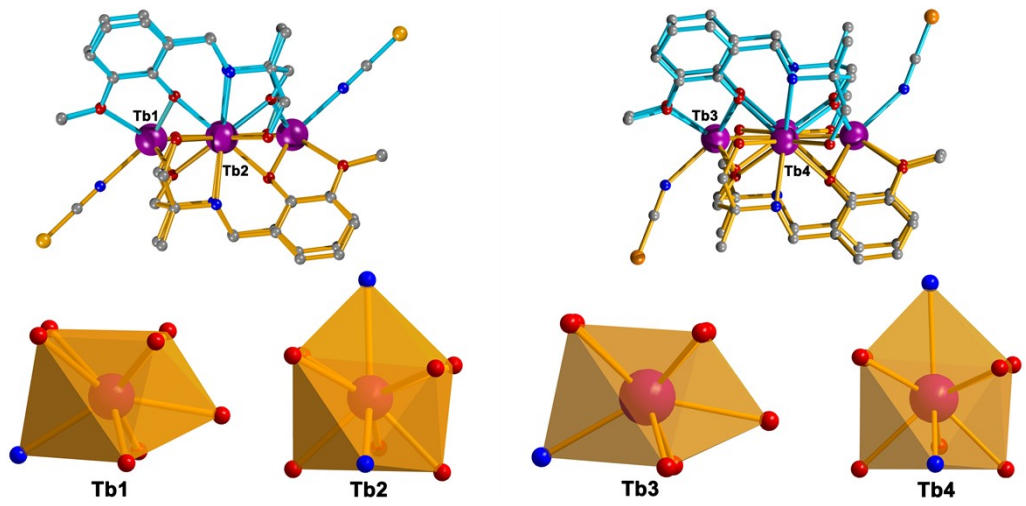


Fig. S1 Side views (top) of the molecule **a** (left) and **b** (right) in complex **1**, with the relevant coordination polyhedron of the Tb<sup>III</sup> centers shown in the bottom.

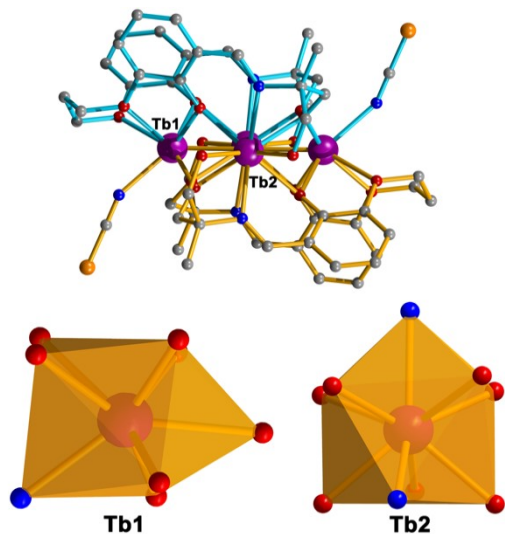


Fig. S2 Side views (top) of complex **2** and the relevant coordination polyhedron of the Tb<sup>III</sup> centers (bottom).

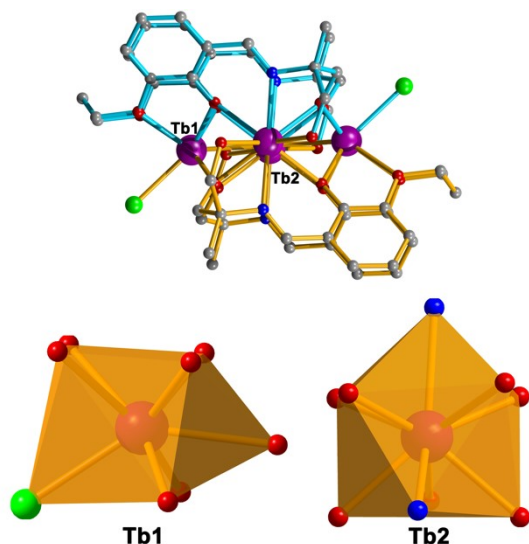


Fig. S3 Side views (top) of complex **3** and the relevant coordination polyhedron of the Tb<sup>III</sup> centers (bottom).

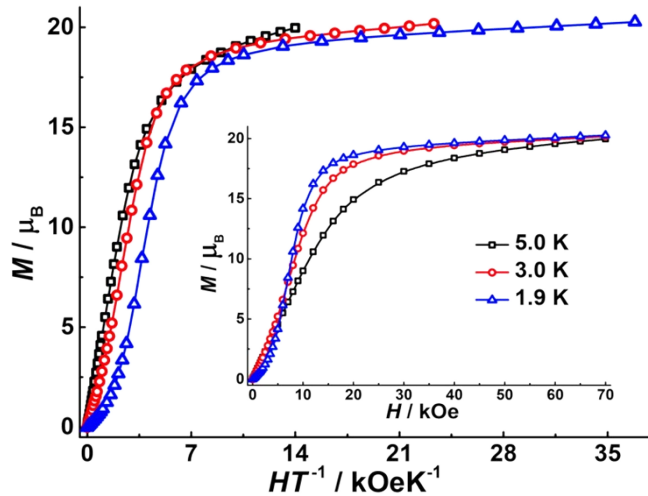


Fig. S4 Molar magnetization ( $M$ ) versus  $H/T$  for **1** at indicated temperatures. Inset represents the plots of magnetization  $M$  versus  $H$ .

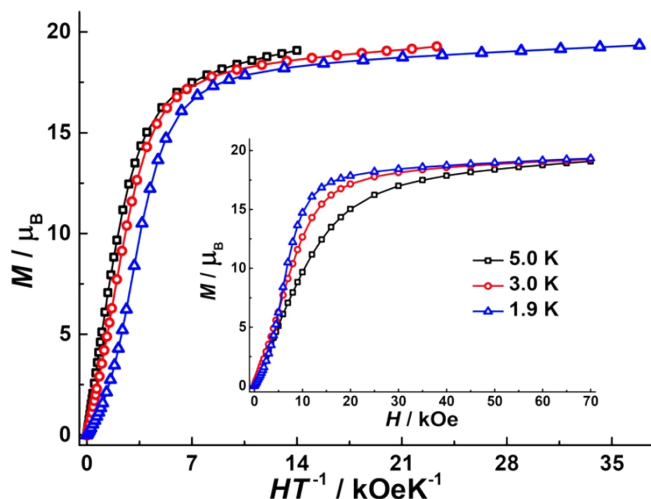


Fig. S5 Molar magnetization ( $M$ ) versus  $H/T$  for **2** at indicated temperatures. Inset represents the plots of magnetization  $M$  versus  $H$ .

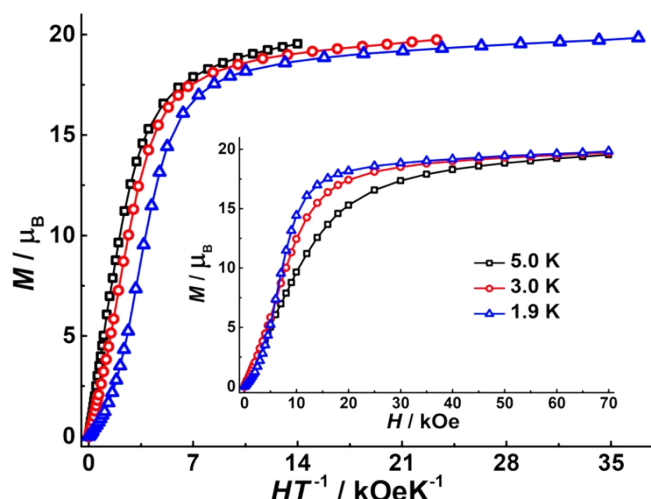


Fig. S6 Molar magnetization ( $M$ ) versus  $H/T$  for **3** at indicated temperatures. Inset represents the plots of magnetization  $M$  versus  $H$ .

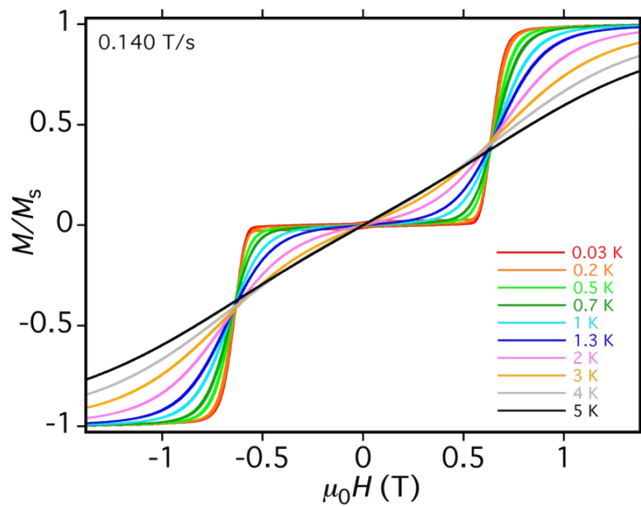


Fig. S7  $M/M_s$  at indicate temperatures for dc field sweep rate of  $0.14 \text{ T}\cdot\text{s}^{-1}$  for complex **1**.

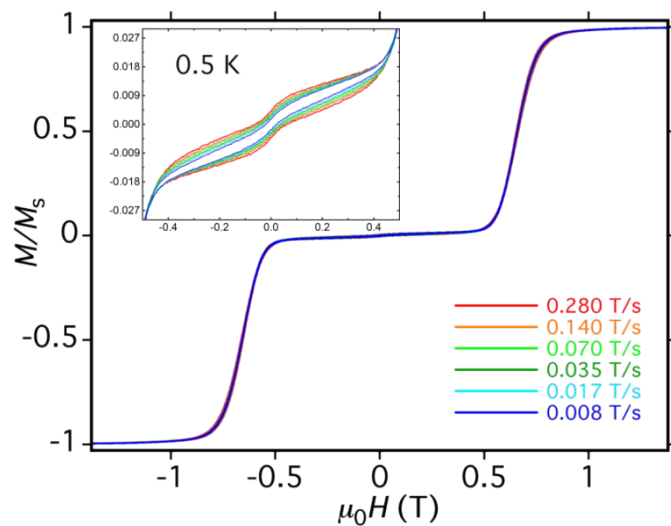


Fig. S8  $M/M_s$  at  $0.5 \text{ K}$  for indicated dc field sweep rate for complex **1**. Insets: zoomed-in plots in the field range of  $-0.5$  to  $0.5 \text{ T}$ .

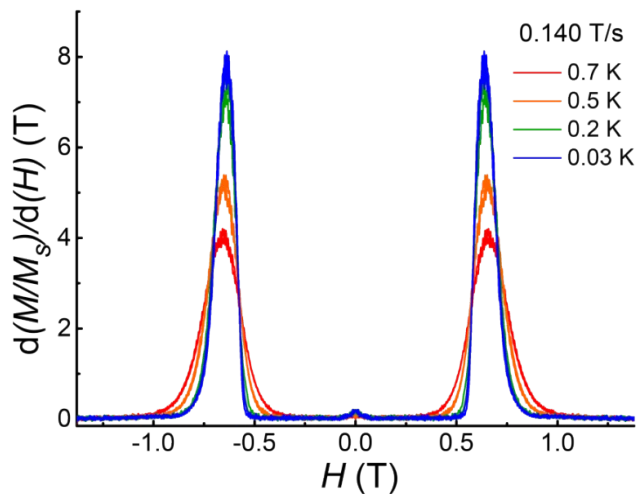


Fig. S9  $d(M/M_s)/dH$  of **1** at different temperatures with dc field sweep rate of  $0.14 \text{ T}\cdot\text{s}^{-1}$ . Quantum tunneling maxima at zero and first resonant fields are observed.

### Ab initio calculations for individual Tb sites in 1, 2 and 3

All calculations were done with OpenMOLCAS<sup>2</sup> (master version of 08 July 2021) and are of CASSCF/RASSI/SINGLE\_ANISO type. The mononuclear Tb<sup>III</sup> fragments have the same structure as the initial **Tb<sub>4</sub>** complex, in which all other three Tb<sup>III</sup> ions were computationally substituted by diamagnetic Lu<sup>III</sup>. VTZP basis sets for Tb<sup>III</sup> and close atoms were used, while smaller VDZ basis sets were used for the distant atoms. Active space of the CASSCF method included 8 electrons in 7 orbitals for Tb (4f orbitals of Tb<sup>III</sup> ion). To exclude all the doubts, we calculated all the roots in the active space. The state-averaged CASSCF orbitals of the septets, quintets, triplets, and singlets were optimized with 7, 126, 308, 197 states, respectively, and mixed by spin-orbit coupling in RASSI.<sup>3</sup> On the basis of the resulting spin-orbital multiplets, SINGLE\_ANISO program computed local magnetic properties (g-tensors, magnetic axes, local magnetic susceptibility, etc.). The magnetic properties of the entire complex, involving four Tb<sup>III</sup> centers were calculated by the POLY\_ANISO program, in which the anisotropic exchange interactions were simulated within the Lines model.

Table S4 *Ab initio* information about individual magnetic centers in the investigated complexes.

Spin-orbit energy states (cm <sup>-1</sup> )							
Molecule <b>a</b> in complex 1		Molecule <b>b</b> in complex 1		Complex 2		Complex 3	
Tb1	Tb2	Tb3	Tb4	Tb1	Tb2	Tb1	Tb2
<b>0.00</b>	<b>0.00</b>	<b>0.00</b>	<b>0.00</b>	<b>0.00</b>	<b>0.00</b>	<b>0.00</b>	<b>0.00</b>
<b>0.12</b>	<b>0.12</b>	<b>0.35</b>	<b>0.13</b>	<b>0.05</b>	<b>0.02</b>	<b>0.09</b>	<b>3.02</b>
<b>170.67</b>	<b>94.87</b>	<b>134.54</b>	<b>93.76</b>	<b>101.76</b>	<b>45.41</b>	<b>121.38</b>	<b>26.59</b>
<b>179.01</b>	<b>96.78</b>	<b>156.17</b>	<b>95.67</b>	<b>105.93</b>	<b>47.23</b>	<b>127.79</b>	<b>29.89</b>
213.62	188.46	165.80	178.70	153.68	<b>98.51</b>	171.79	<b>40.16</b>
230.48	196.91	203.69	188.51	172.21	<b>99.75</b>	193.47	<b>46.75</b>
306.26	291.00	273.62	277.60	229.51	149.91	259.06	<b>73.94</b>
349.69	306.34	328.81	292.89	260.10	171.37	279.19	<b>93.27</b>
372.73	367.66	340.72	353.10	297.50	214.56	316.79	130.21
488.76	450.92	449.63	426.75	324.86	232.41	329.86	150.31
498.15	470.94	459.26	446.95	330.05	256.82	343.08	169.23
706.10	600.90	653.27	577.39	381.27	343.39	401.02	294.75
707.79	604.34	654.64	580.45	390.19	346.77	410.80	296.36
...	...	...	...	...	...	...	...
<i>g<sub>z</sub></i> value of the ground doublet state							
17.737	17.729	17.569	17.775	17.168	17.780	17.380	15.969
Angle between <i>g<sub>z</sub></i> axes of the two Tb sites (in degrees)							
89.40		89.32		71.16		67.63	

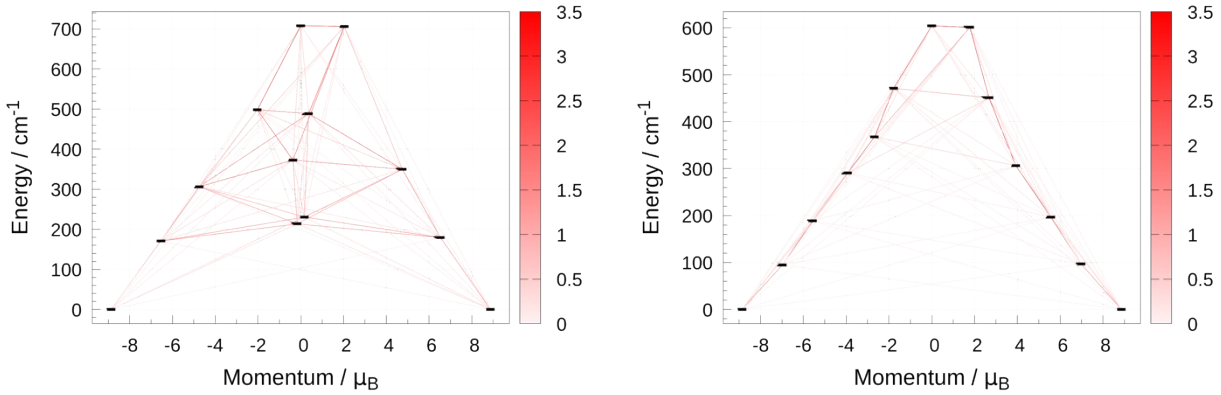


Fig. S10 Energy vs momentum for the ground  $J = 6$  of Tb in the molecule **a** in **1**. The intensity of the red lines indicates the amplitude of the average transition magnetic dipole moment in  $\mu_B$  between the connected states (see the legend in the right-hand side), the square of which roughly scales with the rate of spin-phonon transition between them. The most intense lines outline the magnetization blocking barrier (solid red lines).

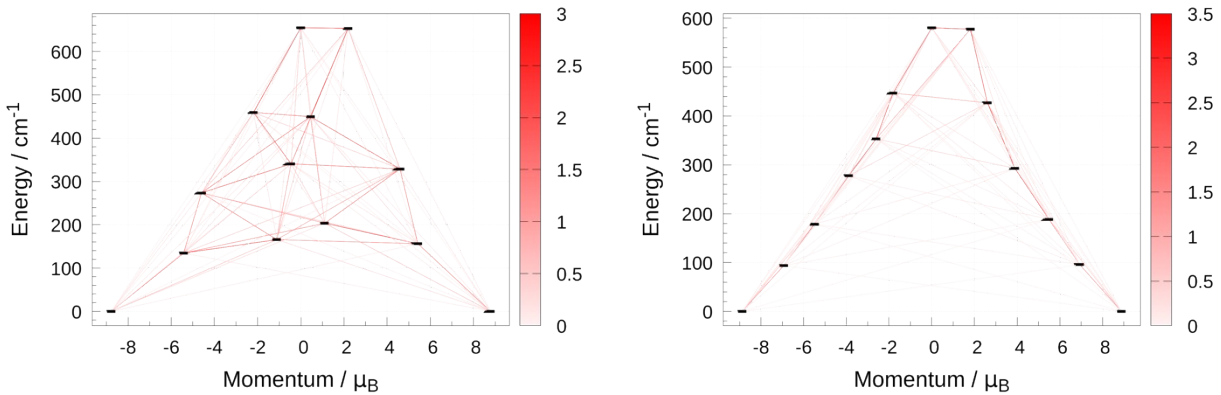


Fig. S11 Energy vs momentum for the ground  $J = 6$  of Tb in molecule **b** in **1**. The intensity of the red lines indicates the amplitude of the average transition magnetic dipole moment in  $\mu_B$  between the connected states (see the legend in the right-hand side), the square of which roughly scales with the rate of spin-phonon transition between them. The most intense lines outline the magnetization blocking barrier (solid red lines).

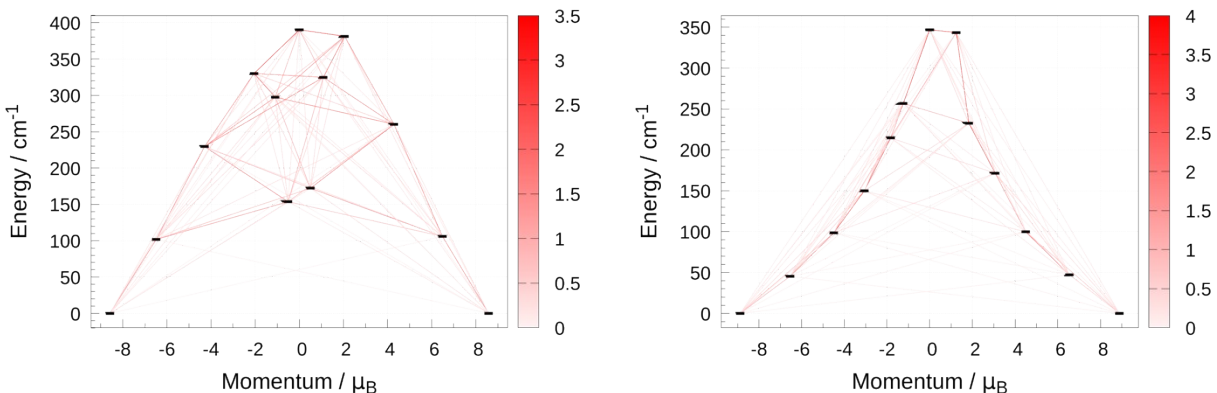


Fig. S12 Energy vs momentum for the ground  $J = 6$  of Tb in complex **2**. The intensity of the red lines indicates the amplitude of the average transition magnetic dipole moment in  $\mu_B$  between the connected states (see the legend in the right-hand side), the square of which roughly scales with the rate of spin-phonon transition between them. The most intense lines outline the magnetization blocking barrier (solid red lines).

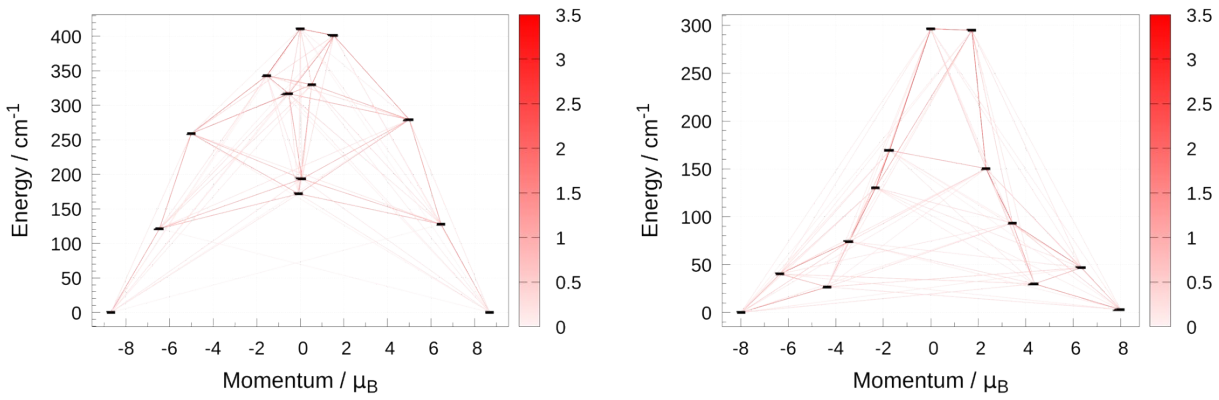


Fig. S13 Energy vs momentum for the ground  $J = 6$  of Tb in complex **3**. The intensity of the red lines indicates the amplitude of the average transition magnetic dipole moment in  $\mu_B$  between the connected states (see the legend in the right-hand side), the square of which roughly scales with the rate of spin-phonon transition between them. The most intense lines outline the magnetization blocking barrier (solid red lines).

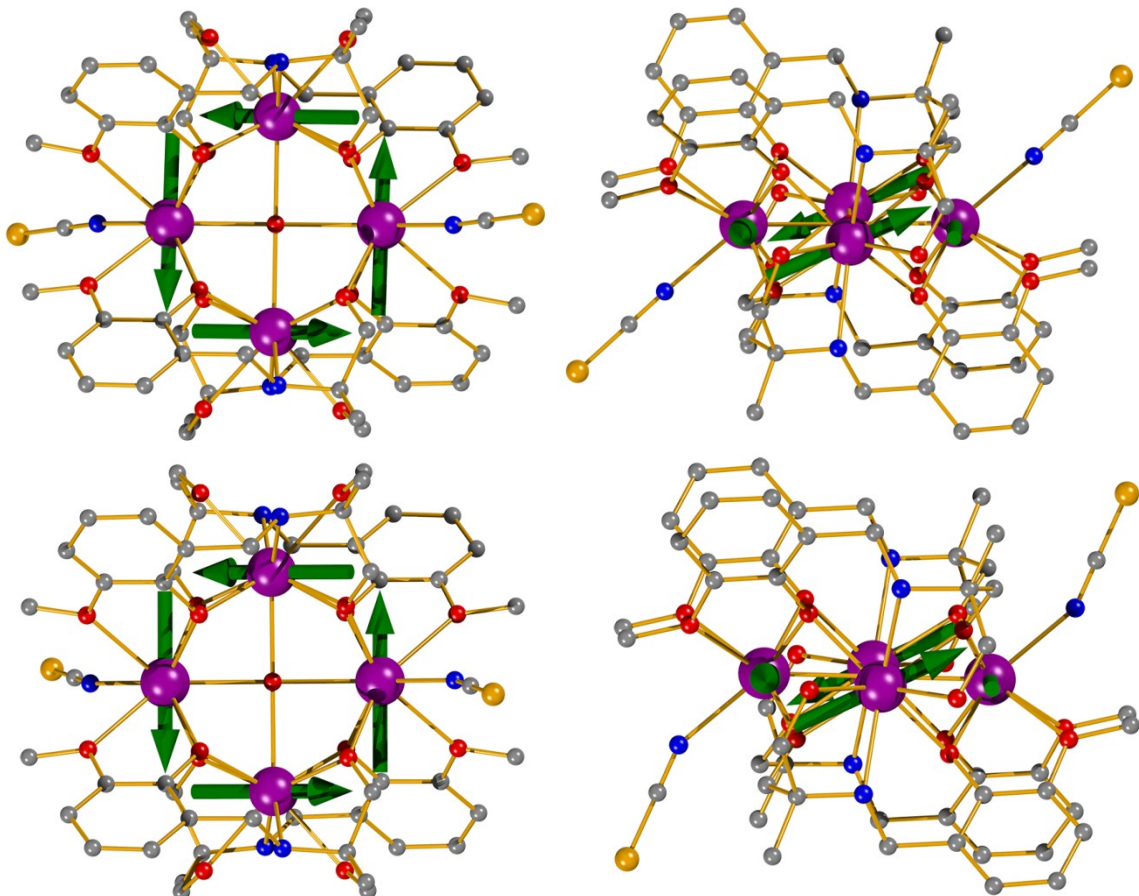


Fig. S14 Top (left) and side (right) views of the orientations of the main magnetic axes and local magnetizations in the ground state of the molecules **a** (top) and **b** (bottom) in complex **1**.

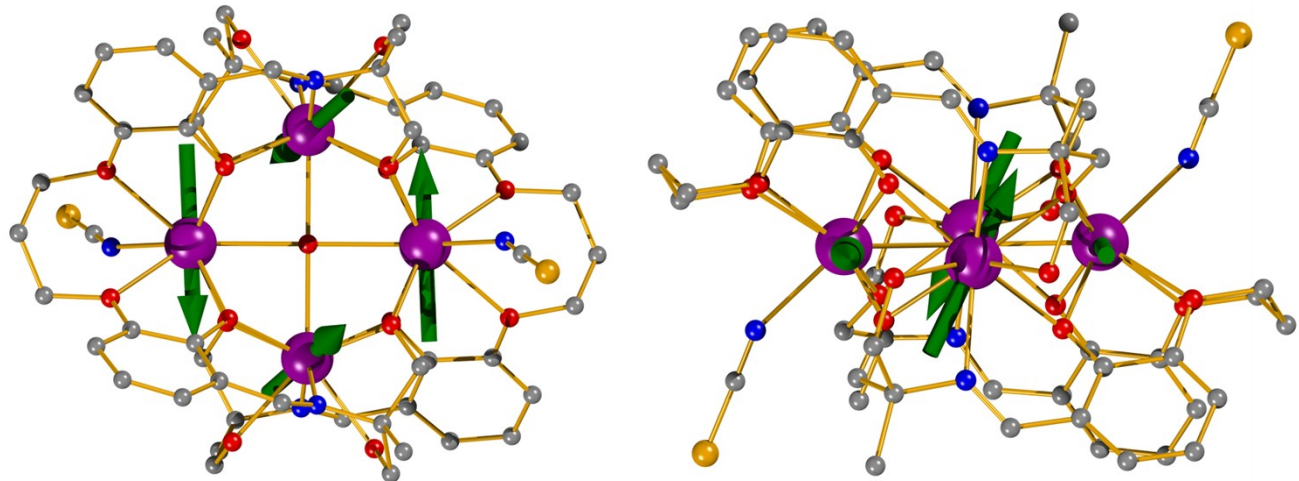


Fig. S15 Top (left) and side (right) view of the orientations of the main magnetic axes and local magnetizations in the ground state of the complex 2.

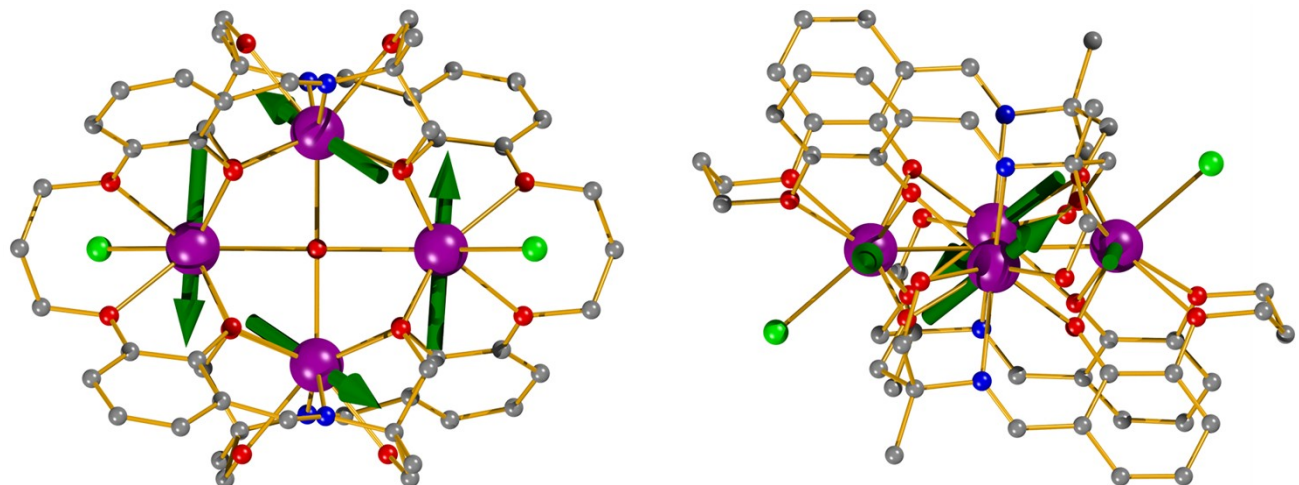


Fig. S16 Top (left) and side (right) view of the orientations of the main magnetic axes and local magnetizations in the ground state of the complex 3.

### Model of the exchange interaction in $\text{Tb}_4$ complex

The magnetic interactions between  $\text{Tb}^{3+}$  ions include contributions from magnetic dipole–dipole and exchange interactions. The exchange coupling was simulated within the Lines model.<sup>4</sup> Magnetic behavior of four interacting  $\text{Tb}^{3+}$  ions was described using a noncollinear Ising Hamiltonian with one coupling constant:

$$\mathcal{H}_{exch} = -J_1 \left( \hat{s}_{Tb_1} \hat{s}_{Tb_2} + \hat{s}_{Tb_1} \hat{s}_{Tb_2^\perp} + \hat{s}_{Tb_2} \hat{s}_{Tb_1^\perp} + \hat{s}_{Tb_1^\perp} \hat{s}_{Tb_2^\perp} \right) - J_2 \left( \hat{s}_{Tb_1} \hat{s}_{Tb_1^\perp} + \hat{s}_{Tb_2} \hat{s}_{Tb_2^\perp} \right) \quad (\text{Eq. 1})$$

where  $s_i$  are projection operators of the effective spin of Tb ions on the corresponding anisotropy axis.  $J_{1,2}$  are the parameters of the inter-site magnetic exchange interaction and represent the only two fitting parameters of the employed model. The inter-site magnetic dipole-dipole interaction is computed using Eq. (2) and added to the exchange Hamiltonian:

$$\hat{H}_{dip}(i,j) = \mu_{Bohr}^2 \times \frac{\hat{\mu}_i \cdot \hat{\mu}_j - 3(\hat{\mu}_i \cdot \hat{n}_{ij})(\hat{\mu}_j \cdot \hat{n}_{ij})}{r_{ij}^3}$$

(Eq. 2)

where  $\hat{\mu}_i$ ,  $\hat{\mu}_j$  are the magnetic moments on the sites  $i$  and  $j$ , respectively, as obtained from the SINGLE\_ANISO single-site calculations,  $\hat{n}_{ij}$  is the normalized vector connecting sites  $i$  and  $j$  (of length = 1),  $r_{ij}$  is the distance between magnetic sites  $i$  and  $j$ , while  $\mu_{Bohr}^2$  is the square Bohr magneton constant, with an approximate value of 0.4329702 cm<sup>-1</sup>/Tesla. The total Hamiltonian of magnetic interaction is a sum of the two operators:

$$\hat{H}_{total} = \hat{H}_{exch} + \hat{H}_{dip}$$

(Eq. 3)

The low-lying energy spectra obtained by diagonalization of the  $\hat{H}_{total}$  and of individual  $\hat{H}_{exch}$  and  $\hat{H}_{dip}$  are given in Table S5. The energy splitting gives a rough estimation on the importance of exchange and dipolar couplings on the total interaction. As such, for the considered Tb<sub>4</sub> the dipole-dipole interaction induces a weaker energy splitting compared to exchange interaction.

The eigenstates of  $\hat{H}_{total}$  are further used for the description of magnetic susceptibility and molar magnetization of the entire tetrานuclear complexes. The parameters  $J_{1,2}$  were found by minimization of the standard deviation function between measured and calculated magnetic susceptibility. Given that the exchange interaction is rather weak and induces weak splitting, only the low-temperature experimental data points, were considered in the fitting. This task was achieved within the POLY\_ANISO code. The best fit gives the coupling values:

Table S5 Energies of the exchange states (cm<sup>-1</sup>) for complex **1a**.

	Molecule <b>a</b> in <b>1</b>	Molecule <b>b</b> in <b>1</b>	Complex <b>2</b>	Complex <b>3</b>
$J_1$	0.391	0.312	0.332	0.119
$J_2$	-0.058	-0.054	-0.160	-0.120

Table S6 Energies of the exchange states (cm<sup>-1</sup>) for molecule **a** in **1**.

Low-lying exchange states (cm <sup>-1</sup> )			
Exchange only	Dipole-dipole only	Total	Total, relative
-0.792884312251	-4.400950553543	-5.416421827810	0.000000000000
-0.775751077089	-4.400944059438	-5.416418261891	0.000003565919
-0.775260817739	0.192884082769	0.131483385914	5.547905213724
-0.758289256822	0.207827283884	0.137773879648	5.554195707458
0.072341142197	0.236583076886	0.158852885788	5.575274713597
0.087902096690	0.237582291100	0.161016804814	5.577438632624
0.184428786253	0.243335254747	0.186280744083	5.602702571893
0.185403603919	0.260070278294	0.190021032986	5.606442860796
0.192973027053	0.273266019553	0.202153853945	5.618575681755
0.200719224826	0.273362023243	0.203364894879	5.619786722688
0.202736565023	0.725097979830	0.659252695415	6.075674523224

0.217817899055	0.730591904748	0.660089513860	6.076511341670
0.328148680173	0.932003048192	2.720919209802	8.137341037612
0.338541934161	0.934599235743	2.721384607469	8.137806435278
2.089560474090	3.821124006181	2.806606936722	8.223028764532
2.089652982135	3.821141196996	2.807088142886	8.223509970696
...	...	...	...

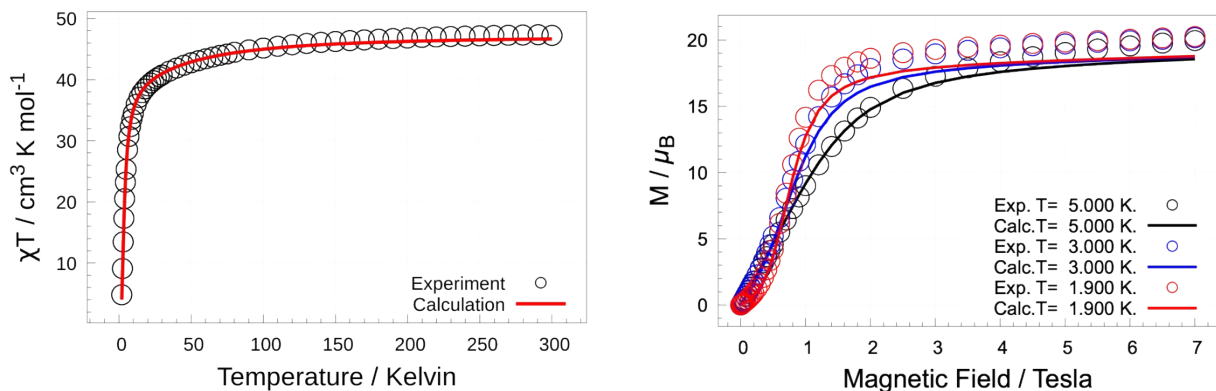


Fig. S17 A comparison between measured and calculated magnetic susceptibility and molar magnetization for molecule **a** in **1**.

Table S7 Energies of the exchange states ( $\text{cm}^{-1}$ ) for molecule **b** in **1**.

Low-lying exchange states ( $\text{cm}^{-1}$ )			
Exchange only	Dipole-dipole only	Total	Total, relative
-0.581882631636	-4.230672902671	-5.154645772964	0.000000000000
-0.560129984073	-4.230619490110	-5.154614828471	0.000030944493
-0.453934629001	0.287889154224	0.289767834933	5.444413607897
-0.433339824151	0.308045728725	0.303917076948	5.458562849912
0.181017558404	0.462913031008	0.417202999189	5.571848772153
0.207846581836	0.476731642064	0.425395418213	5.580041191176
0.427898259747	0.486807349449	0.430580591517	5.585226364481
0.445755769175	0.491831396413	0.437538262327	5.592184035291
0.448800459640	0.495516511590	0.438545000353	5.593190773317
0.469395330545	0.500980135092	0.445614050109	5.600259823073
0.525949917662	1.009817857514	1.025151387930	6.179797160894
0.572544749020	1.037014523804	1.029572708132	6.184218481096
0.716941109558	1.238309790761	2.820104135476	7.974749908440
0.739589641308	1.252048172866	2.820897336411	7.975543109375
2.224071927905	4.135926403839	3.215591458794	8.370237231758
2.225083904855	4.136064229905	3.216535328450	8.371181101414
...	...	...	...

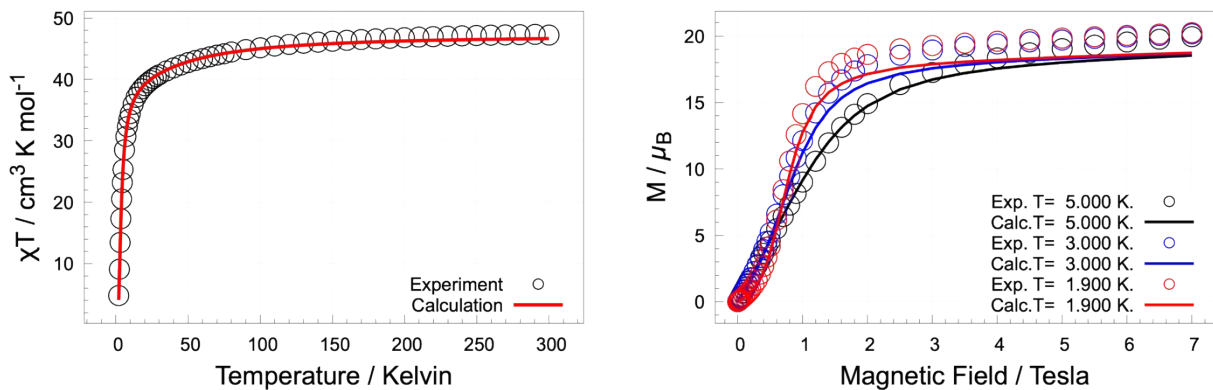


Fig. S18 A comparison between measured and calculated magnetic susceptibility and molar magnetization for molecule **b** in **1**.

Table S8 Energies of the exchange states ( $\text{cm}^{-1}$ ) for complex **2**.

Low-lying exchange states ( $\text{cm}^{-1}$ )			
Exchange only	Dipole-dipole only	Total	Total, relative
-2.610888339558	-2.195612797369	-4.887870013109	0.000000000000
-2.610716547013	-2.195612266138	-4.887869949946	0.00000063162
-2.608650521029	-0.013532608358	-1.199877492973	3.687992520136
-2.608478924853	-0.013232423668	-1.199867427929	3.688002585180
-0.996991315532	0.011741783361	-1.052878584265	3.834991428844
-0.996988800040	0.011852975750	-1.052864786732	3.835005226377
-0.105407147596	0.069294486763	-0.075430585425	4.812439427684
-0.105110547924	0.069772469708	-0.075201752100	4.812668261009
-0.104244988741	0.138140541052	-0.073839152875	4.814030860234
-0.103953342199	0.138583001642	-0.073622111274	4.814247901835
0.095531970891	0.142873897216	0.032358959083	4.920228972192
0.095859700783	0.143606962471	0.032826741005	4.920696754114
0.096634905159	0.951278183732	0.033489816295	4.921359829404
0.096965246410	0.951279715897	0.033965707452	4.921835720561
6.190372069694	1.496515288289	7.049207113024	11.937077126133
6.190372091923	1.496518971478	7.049207128140	11.937077141249
...	...	...	...

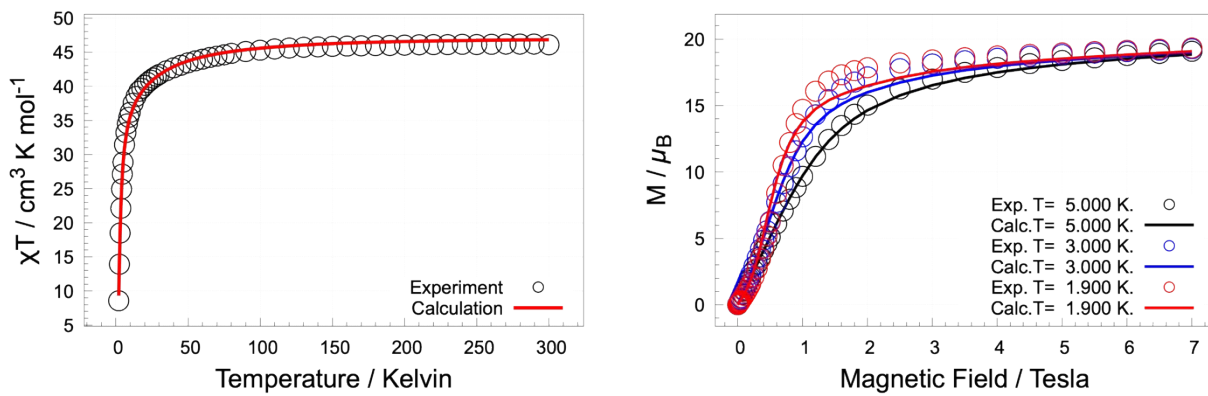


Fig. S19 A comparison between measured and calculated magnetic susceptibility and molar magnetization for **2**.

Table S9 Energies of the exchange states ( $\text{cm}^{-1}$ ) for complex **3**.

Low-lying exchange states ( $\text{cm}^{-1}$ )			
Exchange only	Dipole-dipole only	Total	Total, relative
-1.025038805101	-1.163074113555	-2.633271865590	0.000000000000
-1.020248324214	-1.158914882796	-2.631973727499	0.001298138091
0.736246917291	0.288869297741	0.796813609723	3.430085475313
0.741135095125	0.292695650040	0.797745160912	3.431017026502
1.272577027357	2.839581902739	1.672094168262	4.305366033852
1.277067258541	2.852786315806	1.677945346830	4.311217212420
2.954266235675	2.954896728777	2.811554242603	5.444826108193
2.958619417501	2.972553052854	2.814929147984	5.448201013574
3.210360292676	3.230897969684	3.288931468269	5.922203333859
3.214850613485	3.243797879154	3.292079003347	5.925350868937
4.617671737093	3.440745061436	4.741316616517	7.374588482107
4.623843033365	3.458410336151	4.746533116788	7.379804982378
5.253641765541	6.373519952618	5.613650733531	8.246922599121
5.254782473045	6.388995894292	5.614470544878	8.247742410468
7.628734639959	6.799404784442	8.106700823539	10.739972689129
7.631595853548	6.814918577921	8.108888498740	10.742160364330
...	...	...	...

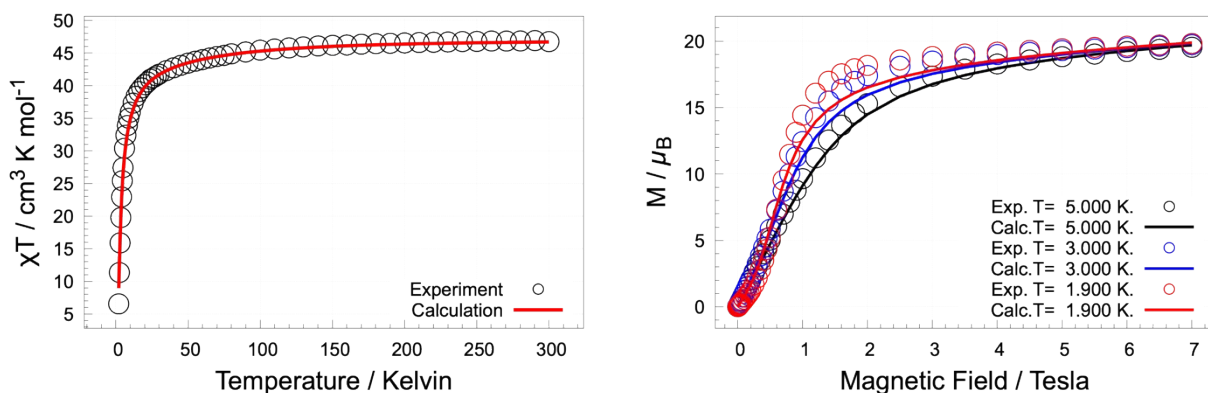


Fig. S20 A comparison between measured and calculated magnetic susceptibility and molar magnetization for **3**.

## References

- 1 a) D. Casanova, M. Llunell, P. Alemany and S. Alvarez, The Rich Stereochemistry of Eight-Vertex Polyhedra: A Continuous Shape Measures Study, *Chem. Eur. J.*, 2005, **11**, 1479-1494; b) D. Casanova, P. Alemany, J. M. Bofill and S. Alvarez, Shape and Symmetry of Heptacoordinate Transition-Metal Complexes: Structural Trends, *Chem. Eur. J.*, 2003, **9**, 1281-1295.
- 2 a) I. Fdez. Galván, M. Vacher, A. Alavi, C. Angeli, F. Aquilante, J. Autschbach, J. J. Bao, S. I. Bokarev, N. A. Bogdanov, R. K. Carlson, L. F. Chibotaru, J. Creutzberg, N. Dattani, M. G. Delcey, S. S. Dong, A. Dreuw, L. Freitag, L. M. Frutos, L. Gagliardi, F. Gendron, A. Giussani, L. González, G. Grell, M. Guo, C. E. Hoyer, M. Johansson, S. Keller, S. Knecht, G. Kovačević, E. Källman, G. Li Manni, M. Lundberg, Y. Ma, S. Mai, J. P. Malhado, P. Å. Malmqvist, P. Marquetand, S. A. Mewes, J. Norell, M. Olivucci, M. Oppel, Q. M. Phung, K. Pierloot, F. Plasser, M. Reiher, A. M. Sand, I. Schapiro, P. Sharma, C. J. Stein, L. K. Sørensen, D. G. Truhlar, M. Ugandi, L. Ungur, A. Valentini, S. Vancoillie, V. Veryazov, O. Weser, T. A. Wesołowski, P.-O. Widmark, S. Wouters, A. Zech, J. P. Zobel and R. Lindh, OpenMolcas: From Source Code to Insight, *J. Chem. Theory Comput.*, 2019, **15**, 5925-5964; b) F. Aquilante, J. Autschbach, A. Baiardi, S. Battaglia, V. A. Borin, L. F. Chibotaru, I. Conti, L. D. Vico, M. Delcey, I. F. Galván, N. Ferré, L. Freitag, M. Garavelli, X. Gong, S. Knecht, E. D. Larsson, R. Lindh, M. Lundberg, P. Å. Malmqvist, A. Nenov, J. Norell, M. Odelius, M. Olivucci, T. B. Pedersen, L. Pedraza-González, Q. M. Phung, K. Pierloot, M. Reiher, I. Schapiro, J. Segarra-Martí, F. Segatta, L. Seijo, S. Sen, D.-C. Sergentu, C. J. Stein, L. Ungur, M. Vacher, A. Valentini and V. Veryazov, Modern quantum chemistry with [Open]Molcas, *J. Chem. Phys.*, 2020, **152**, 214117.
- 3 a) B. O. Roos, P. R. Taylor and P. E. M. Siegbahn, A complete active space SCF method (CASSCF) using a density matrix formulated super-CI approach, *Chem. Phys.*, 1980, **48**, 157-173; b) P.-Å. Malmqvist and B. O. Roos, The CASSCF state interaction method, *Chem. Phys. Lett.*, 1989, **155**, 189-194.
- 4 M. E. Lines, Orbital Angular Momentum in the Theory of Paramagnetic Clusters, *J. Chem. Phys.*, 1971, **55**, 2977-2984.